Li, J., Naafs, B. D. A., Pancost, R. D., Yang, H., Liu, D., & Xie, S. (2017). Distribution of branched tetraether lipids in ponds from Inner Mongolia, NE China: Insight into the source of brGDGTs. *Organic Geochemistry*, *112*, 127-136. https://doi.org/10.1016/j.orggeochem.2017.07.005

Distribution of branched tetraether lipids in ponds from Inner Mongolia, NE China: Insight into the source of brGDGTs

Jingjing Li[a,b,c,d], B. David A. Naafs[c,d], Richard D. Pancost[c,d], Huan Yang[b], Deng Liu[b], Shucheng Xie[b*]

[a] *State Key Laboratory of Lake Sciences and Environment, Nanjing Institute of Geography and Limnology, Chinese Academy of Sciences, Nanjing 210008, China*

[b] *State Key Laboratory of Biogeology and Environmental Geology, School of Earth Sciences, China University of Geosciences, Wuhan 430074, China*

[c] *Organic Geochemistry Unit, School of Chemistry, University of Bristol, Bristol BS8 1TS, UK*

[d] *Cabot Institute, University of Bristol, Bristol BS8 1TH, UK*

* Corresponding author. Tel.: +86 13554116626.

E-mail address: xiecug@163.com (S. Xie).

ABSTRACT

We examined the distributions of branched glycerol dialkyl glycerol tetraethers (brGDGTs) in surface sediments and associated catchment soils of 11 Inner Mongolian ponds (NE China) that collectively comprise a salinity gradient. From this, we explored the sources of brGDGTs in the surface sediments, specifically the source of newly identified brGDGT isomers. Comparative analysis of brGDGT distribution between surface sediments and soils indicated that the proportion of brGDGTs produced *in situ* within ponds was relatively minor compared with that contributed from catchment soils. The sole exception was the recently identified 6-Me hexamethylated brGDGT (IIIa') isomer, which in the surface sediments appeared to be significantly produced *in situ* or in the water column. However the 6-Me pentamethylated brGDGT (IIa') isomer was derived primarily from the surrounding soils based on the plot of individual brGDGT isomers. By extension, the brGDGT-IIIa' and -IIa' components in surface sediments have different biological sources but in soils share a similar biological source.

1. Introduction

Glycerol dialkyl glycerol tetraethers (GDGTs, Fig. 1) are membrane-spanning core lipids synthesized by Archaea and some Bacteria and are ubiquitous in soils, sediments and associated geological archives. Their biological and geochemical occurrence, as well as the application of GDGT-based proxies to past environmental reconstruction, has recently been reviewed by Schouten et al. (2013). Branched GDGTs (brGDGTs; (Sinninghe Damsté et al., 2000) are derived from Bacteria and were initially identified in peat, soil and lake sediments (Schouten et al., 2000; Sinninghe Damsté et al., 2000). BrGDGTs feature methylated *n*-alkyl chains containing up to two cyclopentane moieties (Fig. 1), comprising three structural groups, namely type I, II and III, respectively (Weijers et al., 2006a; 2006b).

Despite the common occurrence of brGDGTs in natural archives, their microbial source is largely unknown. There are no cultured organisms reported to produce abundant brGDGTs, except for three subdivisions (SD 1, 3 and 4) of the bacterial phylum *Acidobacteria* that synthesize a small amount of brGDGT-Ia (Sinninghe Damsté et al., 2011; 2014). However, several studies of terrestrial hot springs suggest that brGDGTs can be produced *in situ* by thermophilic bacteria (Hedlund et al., 2013; Zhang et al., 2013). Recently, the phyla *Proteobacteria* and *Bacteroidetes* were proposed as a biological source of brGDGTs on the basis of comparative analysis of bacterial 16S rRNA

gene sequences and the methylation index of brGDGTs (Li et al., 2014).

The "MBT-CBT" proxy is based on the distribution of brGDGTs, using a combination of the methylation of branched tetraethers (MBT) and the cyclization of branched tetraether (CBT) indices. In a global mineral soil dataset, MBT/CBT was shown to correlate with mean annual air temperature (MAAT) and soil pH (Weijers et al., 2007), a relationship subsequently revised as MBT'-CBT, which excluded brGDGT-IIIb and -IIIc (Peterse et al., 2012). Recently, regional soil calibrations have been proposed for semiarid and arid regions of China (Yang et al., 2014). However, due to the difference in brGDGT distributions in lake sediments and surrounding soils (Sinninghe Damsté et al., 2009; Tierney and Russell, 2009), application of the soil-based MBT-CBT calibration to lake surface sediments generally underestimates observed temperatures (Bechtel et al., 2010; Loomis et al., 2011). Following this discovery, several global and regional lake-specific temperature calibrations were generated (Tierney et al., 2010; Pearson et al., 2011; Sun et al., 2011; Loomis et al., 2012; Günther et al., 2014). Despite the widespread application of lake-specific MBT-CBT calibrations in limnology (Das et al., 2012; Woltering et al., 2014), the complex range of possible brGDGT sources, including catchment soils, rivers and *in situ* production in either lake waters or sediments, significantly complicates their application as a (lake) palaeothermometer (Sinninghe Damsté et al., 2012; Zell et al., 2013; Buckles et al., 2014a; Loomis et al., 2014b; Li et al., 2016).

Recently, new sets of structural isomers that differ in the position of methyl groups on the two C_{28} alkyl chains and co-elute with traditional brGDGTs have been identified (De Jonge et al., 2013; 2014a; 2014b). These new compounds are characterized by methyl groups at the α-6 (or ω-6) position (6-methyl or 6-Me brGDGTs) instead of the classical α-5 (or ω-5) position (5-methyl or 5-Me brGDGTs; Fig. 1) (Weijers et al., 2006a; De Jonge et al., 2013). Subsequently, the abundance and variability of these new brGDGT isomers have been determined for a set of globally distributed mineral soils (De Jonge et al., 2014a; Xiao et al., 2015; Yang et al., 2015; Dang et al., 2016b; Naafs et al., 2017a), peat (Naafs et al., 2017b), river and lacustrine settings (De Jonge et al., 2014b; 2015a; Dang et al., 2016a) as well as marine settings (De Jonge et al., 2015b). pH regulates the fractional abundance of 5- vs. 6-Me brGDGTs in both mineral soils (De Jonge et al., 2014a; Naafs et al., 2017a) and peat (Naafs et al., 2017b), new indices such as CBT_{5ME} and CBT' with improved correlations with pH, were introduced. In addition, the recently defined MBT'_{5ME} index has a better correlation with MAAT and a smaller error, and removed the pH dependence compared with the original MBT' (Peterse et al., 2012). Multilinear regression models (MAT_{mr} and MAT_{mrs}) were established and improved the correlation between brGDGT distribution and MAAT (De Jonge et al., 2014a). Naafs et al. (2017a) recently combined all published brGDGT data from mineral soils and demonstrated that excluding samples with a high relative abundance of 6-methyl brGDGTs over 5-methyl brGDGTs led to an improved temperature calibration.

The occurrence and distribution of bacterial GDGTs in a wide variety of lacustrine settings have been investigated extensively (Tierney et al., 2010; Loomis et al., 2011; Sun et al., 2011; Das et al., 2012; Wang et al., 2012; Schoon et al., 2013; Shanahan et al., 2013; Ajioka et al., 2014; Colcord et al., 2015), including the water column (Woltering et al., 2012; Buckles et al., 2014a; 2014b; Loomis et al., 2014b). However, previous lake studies are related to deeper water systems and fewer focused on shallow system with water depth < 1 m. Here we report the distribution of bacterial brGDGTs and the recently assigned isomers in surface sediments and associated catchment soils, from 11 ponds from Inner Mongolia representing a salinity gradient of 1-280 ‰. We use this to unravel the sources of brGDGTs and their isomers in surface sediments from saline ponds and explore their utility in environmental investigations of such settings.

2. Material and methods

2.1. Study locations

The location of sampling sites is shown in Fig. 2 and given in Table 1. The ponds were selected on the basis of a survey of Chinese and Inner Mongolian saline lakes (Zheng et al., 1992; 2002). The ponds are in New Barag Left Banner of Inner Mongolia, NE China. In general, they are relatively small (1.5 – 7.0 km^2 surface area) and shallow (0.2 – 0.5 m water depth). All developed in the mid to late Holocene (Zheng et al., 1992) and normally do not dry-up during the year. According to records of the local Meteorological

Station, during the period from 1971 to 2013 the mean annual temperature in the area was 0.4 °C and the mean annual minimum and maximum temperature values are ca. –5.1 and 6.7 °C, respectively; the mean annual precipitation is ca. 284 mm (http://cdc.nmic.cn/home.do). Annual precipitation is greatly exceeded by evaporation, causing the high salinity of the lakes and ponds (Zheng et al., 1992). Local meteorological station records also indicate that the area is characterized by a semi-arid desert steppe climate. There are hundreds of lakes and ponds distributed in this area, and most of them are created by wind erosion. The water supply of these shallow water bodies is from precipitation and river run-off and the water volume and water level varies between seasons (Zheng et al., 1992). The land use in New Barag Left Banner is grassland for cattle feeding, and the vegetation type at the study site is dominated by C_3 vegetation, mainly *Leymus chinensis*, *Bromus inermis*, *Elytrigia repens*. Typical soils in the area are chernozem, castanozem and meadow soil. We did not measure the soil pH, the soil pH information is obtained from China soil database (http://vdb3.soil.csdb.cn/), with an average pH of 8.0.

2.2. *Sampling*

Eleven surface sediments (0-2 cm) from the deepest point in each pond and eleven soil samples (0-2 cm) were collected during a field campaign in August 2013. Water samples were collected above the surface sediment and sealed in sterile tubes. The

131 concentrations of cations (Na, K, Mg, Ca) and anions (Cl^-, SO_4^{2-}, HCO_3^-, CO_3^{2-}) were
132 measured in the lab after filtering through a 0.22 μm filter and using inductively
133 coupled plasma-optical emission spectrometry (ICP-OES; Thermofisher ICAP6300) for
134 the cations and dionex ion chromatography for the anions. All values represent the
135 mean of duplicate measurements. Salinity was calculated as the sum of the measured
136 ions (Table 1).
137
138 *2.3. Total organic carbon (TOC) and lipid analysis*
139 The method for TOC content analysis has been reported in Li et al. (2016). In general,
140 it was measured by subtracting the inorganic carbon content from the total elemental
141 carbon content, determined using a Carlo Erba EA1108 Elemental Analyzer and
142 modified Coulomat 702 analyser, respectively. All TOC measurements were performed
143 in duplicate.
144 Surface sediment of ponds and soil samples were freeze-dried and ground to powder
145 using a mortar and pestle after transport to the laboratory. Sediment and soil samples
146 (ca. 10 g) were extracted with a mixture of dichloromethane and methanol (DCM/MeOH,
147 2:1 v/v) in pre-cleaned cellulose extraction thimble using Soxhlet apparatus for 24 h
148 (Naafs and Pancost, 2014). An aliquot (50 %) of the total lipid extract was separated
149 over activated Al_2O_3 into an apolar and a polar fraction using hexane:DCM (9:1 v/v) and
150 DCM:MeOH (1:2 v/v), respectively.

151 The polar fraction, containing GDGTs, was dissolved in DCM and filtered through a
152 0.45 um PTFE filter and the solvent removed under a N_2 stream. GDGTs were analyzed
153 using high performance liquid chromatography-mass spectrometry (HPLC-MS^2; Agilent
154 1200), with auto-injection and ChemStation manager software. The sample was
155 re-dissolved in hexane/isopropanol (99:1 v/v) and an internal synthetic C_{46} standard
156 (Huguet et al., 2006) was added for quantification. The occurrence of 5- and 6-Me
157 isomers of hexa- and penta-methylated brGDGTs has been investigated in peat (De
158 Jonge et al., 2013; Naafs et al., 2017b), mineral soil (De Jonge et al., 2014a; Yang et al.,
159 2015; Dang et al., 2016b), as well as in lacustrine and marine sediments and water
160 column (De Jonge et al., 2015a; 2015b; Weber et al., 2015; Dang et al., 2016a) using
161 Prevail or Alltima silica columns. Here we used a Thermo Finnigan silica column (150
162 mm × 2.1 mm, 1.9 um) to separate the 5- and 6-Me hexa- and penta-methylated
163 brGDGTs (Supplementary Fig. 1). Injection volume was 10 μl. The elution gradient
164 follows the procedure of Yang et al. (2014) with some modifications. It first eluted
165 isocratically (5 min) with 80% A and 20% B, where A = hexane and B =
166 hexane/isopropanol (9:1 v/v), followed by changing the ratio to 72% A and 28% B from
167 5 to 45 min and then to 70% A and 30% B for 1 min, washing the column with 100% B
168 for 5 min, and then 80% A and 20% B to equilibrate the column. The flow rate was 0.2
169 ml/min. Detection of GDGTs was achieved using single ion monitoring (SIM) of $[M+H]^+$
170 ions, targeting *m/z* 744 for the C_{46} standard, *m/z* 1292 for crenarchaeol, and *m/z* 1050,

1048, 1046, 1036, 1034, 1032, 1022, 1020 and 1018 for the regular brGDGTs. The 5- and 6-Me brGDGT isomers were assigned as described by De Jonge et al. (2014b), and were identified by integration of peak area in the extracted ion chromatograms. Quantification was semi-quantitative as we assumed the ionization efficiency and the relative response factor between brGDGTs and the C_{46} GDGT standard to be similar. The concentration of brGDGTs was then normalized to TOC.

2.4. GDGT-based indices

The 6-Me brGDGTs are denoted by an accent to differentiate the corresponding 5-Me brGDGTs. The isomer ratio (IR_{χ}), following De Jonge et al. (2014b) with some simplification, represents the fractional abundance of the 6-Me penta- and hexamethylated brGDGTs, compared with the total corresponding 5-Me and 6-Me penta- and hexamethylated brGDGTs, where χ represents the 5-Me brGDGT and χ' its corresponding 6-Me isomer. With the Roman numerals referring to the GDGT structures indicated in Fig. 1; a, b, c indicate brGDGTs containing no, one or two cyclopentane moieties, respectively:

$$IR_{IIIa'} = IIIa'/(IIIa + IIIa') \quad (1)$$

$$IR_{IIa'} = IIa'/(IIa + IIa') \quad (2)$$

$$IR_{6me} = (IIa' + IIb' + IIc' + IIIa' + IIIb' + IIIc')/(IIa + IIa' + IIb + IIb' + IIc + Ic' + IIIa + IIIa' + IIIb + IIIb' + IIIc + IIIc') \quad (3)$$

191 The MBT' and CBT indices, which represent the degree of methylation and cyclization,
192 were calculated following Peterse et al. (2012):
193 $MBT' = (Ia + Ib + Ic)/(Ia + Ib + Ic + IIa + IIa' + IIb + IIb' + IIc + IIc' + IIIa + IIIa')$
194 (4)
195 $CBT = -\log[(Ib + IIb + IIb')/(Ia + IIa + IIa')]$ (5)
196 The recently defined MBT'_{5ME} and CBT_{5ME} indices were calculated on the basis of
197 5-Me brGDGTs (De Jonge et al., 2014a):
198 $MBT'_{5ME} = (Ia + Ib + Ic)/(Ia + Ib + Ic + IIa + IIb + IIc + IIIa)$ (6)
199 $CBT_{5ME} = -\log[(Ib + IIb)/(Ia + IIa)]$ (7)
200 Similar to the 5-Me brGDGTs, MBT'_{6ME} and CBT_{6ME} indices based on 6-Me brGDGTs
201 can also be calculated (Yang et al., 2015):
202 $MBT'_{6ME} = (Ia + Ib + Ic)/(Ia + Ib + Ic + IIa' + IIb' + IIc' + IIIa')$ (8)
203 $CBT_{6ME} = -\log[(Ib + IIb')/(Ia + IIa')]$ (9)
204 The BIT index was calculated according to Hopmans et al. (2004) and reflects the
205 relative abundance of bacterial brGDGTs versus crenarchaeol, derived from
206 Thaumarchaeota (Sinninghe Damsté et al., 2002).
207 $BIT = (Ia + IIa + IIIa + IIa' + IIIa')/(Ia + IIa + IIIa + IIa' + IIIa' + Cren)$ (10)
208 We summed the 5- and 6-Me brGDGTs and Cren refers to crenarchaeol.
209
210 *2.5. Statistical analysis*

211 Redundancy analysis (RDA) was performed on the dataset as it could directly
212 visualize the variation in the brGDGTs in relation to environmental variables. The
213 fractional abundance of crenarchaeol and brGDGTs as well as brGDGT-based indices as
214 response variables and water chemistry parameters as explanatory variables were
215 transferred into the Canoco software. The detrended correspondence analysis (DCA)
216 was performed first to measure the lengths of variances, but all of these lengths were <
217 1; therefore, an RDA analysis based on a linear ordination method was selected to
218 process the dataset instead. RDA analysis was performed using the software Canoco for
219 Windows version 4.5.
220
221 **3. Results**
222 *3.1. Water parameters*
223 The pH of the eleven ponds varied from 7.7 to 9.9 and the salinity from 0.8‰ to 279‰
224 (Table 1). Chemical parameters are listed in Table 1. The lowest pH and highest salinity
225 were observed for IM7.
226
227 *3.2. Concentrations of crenarchaeol and brGDGTs in sediments and soils*
228 A typical brGDGT distribution in surface sediments and soils is illustrated in Fig. 3.
229 The TOC-normalized (semi-quantitative) concentrations of crenarchaeol and total
230 brGDGTs and the relative abundance of individual brGDGTs, including the 5- and 6-Me

231 brGDGTs of tetra-, penta- and hexa- methylated brGDGTs are summarized
232 (Supplementary Table 1). The concentration of crenarchaeol in surface sediments was
233 lower than in soils. In surface sediments it ranged between 0.04 and 10 ng/g TOC, with
234 the highest value at IM8. In soils, the concentration ranged from 0.04 to 80 ng/g TOC
235 with the highest value in the soils surrounding (IM5).

236 The concentration of brGDGTs was highly variable, but it was almost always higher in
237 soils than the corresponding surface sediments, varying from 0.3 to 2,100 ng/g TOC for
238 soils and 0.7 to 100 ng/g TOC for the sediments (Supplementary Table 1). BIT index
239 values were similar between surface sediments and soils, ranging from 0.66 to 0.97 in
240 sediments and 0.62 to 0.96 in soils. Generally similar BIT values were observed in
241 surface sediments and corresponding soils (Supplementary Table 2; r^2 0.52 for direct
242 comparison of sediment BIT to corresponding soil).

243

244 *3.3. Distributions of brGDGTs*

245 As illustrated in Supplementary Table 1 and Fig. 3, the brGDGT distributions of both
246 soils and surface sediments were dominated by brGDGTs containing no cyclopentane
247 moieties. Among these, the pentamethylated brGDGTs (IIa and IIa') were generally the
248 most abundant, followed by hexamethylated (IIIa and IIIa') and tetramethylated (Ia)
249 brGDGTs. The relative abundance of summed IIa and IIa' varied from 30 to 50% of total
250 brGDGTs in sediments, whereas it varied between 35 and 60% in soils. The exception of

IM3 sediment, where the fractional abundance of summed IIIa and IIIa' (55%) was higher than that of IIa and IIa' (30%) (Supplementary Table 1). These observations persisted even when only the 5-Me components were considered, i.e. IIa was almost always more abundant than IIIa.

The abundance of IIIa' was generally higher than its isomer IIIa, both in surface sediments and soils (Supplementary Table 1 and Fig. 3). In contrast, the abundance of IIa' (25%) was higher than IIa (17%) in sediments, but lower in soils (20% vs. 29%, respectively). The relative abundance of 6-Me brGDGTs over 5-Me brGDGTs (IR_{6me}) in the mineral soil samples varied between 0.1 and 0.8 with an average of 0.4. Two soils had an IR_{6me} > 0.5. In summary, surface sediments and soils generally had similar brGDGT distributions, with type II the most abundant component; however, the predominance of IIa and IIa' differed between sediments and soils.

3.4. MBT' and CBT values

Average MBT' values were 0.24 ± 0.07 for soils and 0.22 ± 0.09 for surface sediments (Supplementary Table 2), with no significant difference (Fig. 5a), which can be further demonstrated by an independent sample *t*-test (t = 0.643; p = 0.528). This similarity was also true for each individual system (Fig. 5b,c). MBT'_{5ME} values were 0.50 ± 0.13 for sediments and 0.38 ± 0.17 for soils (shown by sample *t*-test, t = 1.907; p = 0.07), whereas MBT'_{6ME} values were 0.32 ± 0.09 and 0.41 ± 0.14 (t = -1.675; p = 0.11),

271 respectively (Supplementary Table 2), reflecting the differences between the II/II' and
272 III/III' components discussed above. The original CBT indices for sediments and soils
273 were 0.68 ± 0.15 and 0.91 ± 0.30 with significant difference (p = 0.04), respectively;
274 CBT_{5ME} values were 0.67 ± 0.20 and 0.95 ± 0.40 (p = 0.05), respectively, and CBT_{6ME}
275 values 0.62 ± 0.16 and 0.75 ± 0.39 (p = 0.36), respectively.
276
277 **4. Discussion**
278 *4.1. Sources of brGDGTs*
279 Previous studies showed that brGDGTs in lacustrine sediments can originate from
280 soils in the catchment area (Weijers et al., 2006b) and rivers (Zell et al., 2013) as well as
281 from *in situ* production within the water column (Sinninghe Damsté et al., 2009;
282 Sinninghe Damsté et al., 2012; Wang et al., 2012; Buckles et al., 2014b; De Jonge et al.,
283 2014b) or sediments (Tierney and Russell, 2009). Unfortunately, we were not able to
284 evaluate the contribution of suspended particulate matter as no water was collected for
285 lipid analysis. Here we compare the fractional abundance and concentration of brGDGTs,
286 as well as the brGDGT-based indices, between surface sediments and soils to evaluate
287 the source of brGDGTs in these (saline) Inner Mongolian ponds.
288
289 *4.1.1. Comparison of brGDGT concentrations between soils and surface sediments*
290 Comparative analysis of brGDGT concentrations indicates that the concentration of

291 brGDGTs is generally higher in soils than in the corresponding surface sediments,
292 except for Pond Targan (Supplementary Table 1). Most other studies have reported a
293 higher concentration of brGDGTs in lake sediments than in associated catchment soils,
294 including Lake Towuti in central Indonesia (Tierney and Russell, 2009), lakes in
295 western Uganda (Loomis et al., 2011), and Sand Pond in Rhode Island, USA (Tierney et
296 al., 2012). The only exception is Lake Cadagno (Switzerland) with similar
297 concentrations of brGDGTs in soil and lake sediment samples (Niemann et al., 2012).
298 The higher abundance of brGDGTs in the Inner Mongolian soils is consistent with them
299 being the primary source of brGDGTs in pond surface sediments. Even if brGDGTs in
300 these small and shallow Inner Mongolian ponds are partly autochthonous, it is likely
301 that soil input dominates the preserved signature; this is consistent with the generally
302 similar brGDGT indices observed in pond sediments and associated soils. A similar
303 results was previously obtained for Lake McKenzie (Woltering et al., 2014).
304 Consequently, it is not surprising that we did not find a relationship between brGDGT
305 concentration in surface sediments and salinity although in general, lake systems with
306 high salinity tend to have larger differences between soil and sediment brGDGT
307 concentration (r^2 = 0.66, Fig. 4).
308
309 *4.1.2. Comparison of distribution patterns of brGDGTs between soils and surface sediments*
310 The brGDGT distributions in surface sediments are similar to those in soils, with

311 brGDGT IIa generally dominating and IIIa also abundant. The dominance of the penta-
312 and hexamethylated brGDGTs over the tetramethylated brGDGTs in our samples from
313 Inner Mongolia, is consistent with the trends in brGDGT distribution of the global
314 mineral soil database with the lowest degree of methylation in mineral soils from polar
315 regions (De Jonge et al., 2014a; Naafs et al., 2017a). The similarity in brGDGT
316 distributions between soils and surface sediments suggests that the former are the
317 major source of the latter, as would be expected for these small and shallow ponds.
318 However, the soils and ponds are exposed to the same climate with similar
319 temperatures and they have a similar pH. Although additional factors such as soil type
320 and vegetation can also influence the brGDGT distribution (Naeher et al., 2014), we
321 cannot rule out the possibility that the distribution of the *in situ* produced brGDGTs in
322 the ponds is similar to that of the surrounding soils. Similar conclusions are derived
323 from the BIT indices, which do not differ markedly between the surface sediments and
324 soils.

325 These observations contrast with previous studies in which MBT' and CBT values
326 were clearly distinct between lake sediments and surrounding soils (Tierney and
327 Russell, 2009; Sun et al., 2011; Wang et al., 2012; Li et al., 2016). We also note that in
328 our previous work, brGDGT distributions in lake sediments from the shallow
329 hypersaline Chaka Salt Lake differed from those in soils, but were similar to those from
330 surrounding river sediments (Li et al., 2016). We attributed that to the very low

concentration of GDGTs in arid and alkaline soils and therefore a dominance of input from more distal highlands. Although the broad features of brGDGT distributions are the same, small differences in the proportions of the 5-Me and 6-Me isomers do exist between surface sediments and soils. This yields differences in the associated indices (Fig. 5), and suggests that some brGDGTs – specifically the 6-Me brGDGTs – are partially produced *in situ* within the ponds. We probe these differences in 5- and 6-Me brGDGTs in the following section.

4.1.3. Autochthonous vs. allochthonous production of 6-Me brGDGTs in surface sediments

The only consistent difference in brGDGT distributions between surface sediments and surrounding soils is that the proportions of IIIa and IIa are lower in the former, whereas those of their respective IIIa' and IIa' isomers are higher (Supplementary Table 1 and Fig. 3). Consequently, the isomer ratios of IIIa' ($IR_{IIIa'}$) and IIa' ($IR_{IIa'}$) are also higher in surface sediments (shown by independent sample *t*-test, $p = 0.065$ for IIIa' and $p = 0.079$ for IIa'), on average. When considering individual surface sediments and corresponding soils, the same relationships are apparent for about half of the ponds, with the rest having similar IIIa' and IIa' ratio values (Fig 6a, b). This suggests that brGDGT-IIIa' and –IIa' in the surface sediments, especially for those ponds where the IIIa' and IIa' ratios were markedly higher, were at least partly produced within the ponds themselves.

It is unclear if such *in situ* production of 6-Me brGDGTs occurs in the water column or sediment, but the former is consistent with the observation of high amounts of brGDGT-IIIa', -IIIb' and –IIIc' in the suspended particulate matter of Yenisei River (De Jonge et al., 2014b). Similarly, the recently identified brGDGT-IIIa'' has been only detected in sediments of Lake Hinterburg but not the surrounding soils (Weber et al., 2015). Note that IIIa'' has not been detected in our Inner Mongolian surface sediment samples, suggesting that it might not be produced in saline ponds.

4.2. Do water salinity, pH and chemical parameters affect brGDGT distributions in surface sediments?

Statistical analysis confirms that pond water pH and salinity have a linear correlation (r^2 0.5, p = 0.02), likely due to the concentration of cations during evaporation. Virtually none of the brGDGT proportions, crenarchaeol abundance, or brGDGT-based indices have a significant correlation with salinity. Only the BIT and CBT_{6ME} indices have weak correlations with salinity (negative with r^2 0.4, p 0.001 and positive with r^2 0.3, p 0.001, respectively). Previous work has shown a strong affect of pH on brGDGT distributions in lacustrine environments (Blaga et al., 2010; Schoon et al., 2013; Loomis et al., 2014a;Wang et al., 2016; Dang et al., 2016a), and the lack of a similar relationship here again suggests that brGDGTs are derived mainly from the surrounding soils.

To test this further, we performed RDA to examine the impact of water variables,

including the Na^+, K^+, Mg^{2+}, Ca^{2+}, Cl^-, SO_4^{2-}, HCO_3^- and CO_3^{2-} concentrations, on the distribution of sedimentary brGDGTs (Fig. 7). In the first RDA dataset (Fig. 7a), axis 1 principally reflects the variation in CO_3^{2-} and axis 2 the variation in HCO_3^-: this exercise confirms the aforementioned analysis, with almost no evidence for a water chemistry control on brGDGT distributions. However, there is a weak positive correlation between the proportion of brGDGT-IIIa and HCO_3^- (r^2 0.5, p 0.001). In the second RDA dataset (Fig. 7b), axis 2 primarily reflects the variation in water chemical parameters (Fig. 7b) and again reveals almost no correlation between them and brGDGT distributions. However, CBT_{6ME} (which includes the proportions of IIa' and IIb') is correlated positively with Mg^{2+}, Ca^{2+} and Cl^-, perhaps providing further evidence that the 6-Me brGDGTs are produced within the ponds, in the water column/sediments.

4.3. Reconstructed MAAT and soil pH based on the soil MBT'/CBT indices

Given little *in situ* production of brGDGTs, we would expect MBT' and CBT-based environmental indices to be relatively robust (i.e. not confounded by the source issues that affect other systems). The global soil-based calibration of Peterse et al. (2012), yields reconstructed MAAT for soils from -2.2 to 8.9 °C, with an average of 2.5 °C, slightly higher but within error of the recorded MAAT of 0.4 °C. The reconstructed soil pH varies from 5.5 to 7.2, with an average of 6.1, lower than the pH of ca. 8. When using the regional calibration for arid/alkaline soil of Yang et al. (2014), the reconstructed

MAAT is higher, ranging from 8.1 to 12.6 °C, with an average of 10.1 °C and markedly higher than recorded MAAT. We also applied the mineral soil calibration established by the separate quantification of 5- and 6-Me brGDGTs (De Jonge et al., 2014a). Using the 5-Me brGDGT-based indices, the reconstructed MAAT varies between -3.3 and 11.7 °C, with an average of 3.4 °C, and the reconstructed pH from 5.2 to 7.1, with an average of 6.2, again inconsistent with the recorded MAAT and pH. The reconstructed temperature based on Index 1 (De Jonge et al. (2014a) ranges from -2.5 to 11.2 °C, with an average of 5.1 °C, again higher and more variable than expected. We further applied the new calibration for arid and/or alkaline soils dominated by 5-methyl brGDGTs (Naafs et al., 2017a). The IR_{6me} in our soil samples averages 0.4, which justifies the use of this particular calibration. The two mineral soil samples with $IR_{6me} > 0.5$ were not used for this calibration. Using this calibration yielded reconstructed temperatures from -7.9 to 10.7 °C , with an average of -1.1 °C, close to the recorded MAAT (0.4 °C). These results indicate that temperature is a primary control on 5-Me brGDGTs. Overall, consideration of more recent calibrations that are either tuned to arid settings or deconvolute the influence of 5-Me and 6-Me isomers fails to yield more accurate MAAT and pH. It is somewhat surprising that the regional soil calibration is not more accurate than the global one, given the arid conditions in the region. It is also surprising that the calibrations of De Jonge et al. (2014a) do not yield more accurate reconstructions given the likely additional sources of 6-Me isomers. Potentially in this particular cold setting,

411 brGDGT-based proxies are biased towards summer seasons when soils are not frozen.
412 The latest mineral soil calibration based on soils dominated by 5-Me brGDGTs only
413 (Naafs et al., 2017a) seems to work well in this area, although the spread in
414 reconstructed MAAT is still large.
415
416 **5. Summary and conclusions**
417 We examined the distributions of brGDGTs in surface sediments and catchment soils
418 of 11 Mongolian ponds comprising a large salinity gradient. We used this to explore the
419 source(s) of brGDGTs, and especially the recently identified 6-Me brGDGTs isomers, in
420 surface sediments. The similarity in brGDGT distributions in surface sediments and
421 catchment soils probably suggests that the former are derived mainly from the
422 surrounding soils. Consistent with this, water characteristics such as salinity and pH,
423 known to influence brGDGT distributions, exhibit no correlation with sedimentary
424 brGDGT distributions in this system. This likely reflects the small size as well as the
425 inhibition of brGDGT production in the higher saline ponds. However, there is evidence
426 that the recently identified 6-Me brGDGTs, and especially the hexamethylated
427 component (IIIa'), are produced both in soils and *in situ* within the pond, potentially
428 providing a guide towards identifying their biological source(s). The majority of the
429 available mineral soil calibrations provide temperatures that are inconsistent with the
430 instrumental temperature record of the region and/or result in a large range of

reconstructed temperature, further highlighting the complex control on the brGDGT distribution in these settings.

Acknowledgments

X. Qiu is thanked for invaluable assistance during the sampling in the field. We would like to thank W.H. Ding, J.T. Xue, W.J. Xiao, R.C. Wang and Y.S. Xue for sample preparation. Dr. Y.H. Zheng is acknowledged for transporting the samples. Dr. Y.X. He is thanked for helpful discussions based on an earlier version of the manuscript and we thank F.F. Zheng for generating the figures. Mr. D. Davis is acknowledged for TOC analysis. Dr. Rienk Smittenberg and an anonymous reviewer are thanked for providing valuable comments on the manuscript. The study was funded by State Key R&D Program of China (Grant No. 2016YFA0601100) and the National Natural Science Foundation of China (Grants No. 41330103 to S.X. and 41502173 to J.L.). R.D.P. and B.D.A.N. acknowledge funding from the advanced ERC Grant "the greenhouse earth system" (T-GRES, project reference 340923).

446

447 **References**

448 Ajioka, T., Yamamoto, M., Murase, J., 2014. Branched and isoprenoid glycerol dialkyl
449 glycerol tetraethers in soils and lake/river sediments in Lake Biwa basin and
450 implications for MBT/CBT proxies. Organic Geochemistry 73, 70-82.

451 Bechtel, A., Smittenberg, R.H., Bernasconi, S.M., Schubert, C.J., 2010. Distribution of
452 branched and isoprenoid tetraether lipids in an oligotrophic and a eutrophic
453 Swiss lake: insights into sources and GDGT-based proxies. Organic Geochemistry,
454 41, 822-832.

455 Blaga, C.I., Reichart, G.-J., Schouten, S., Lotter, A.F., Werne, J.P., Kosten, S., Mazzeo, N.,
456 Lacerot, G., Sinninghe Damsté, J.S., 2010. Branched glycerol dialkyl glycerol
457 tetraethers in lake sediments: Can they be used as temperature and pH proxies?
458 Organic Geochemistry 41,1225-1234.

459 Buckles, L., Weijers, J., Tran, X.-M., Waldron, S., Sinninghe Damsté, J., 2014a. Provenance
460 of tetraether membrane lipids in a large temperate lake (Loch Lomond, UK):
461 implications for glycerol dialkyl glycerol tetraether (GDGT)-based
462 palaeothermometry. Biogeosciences 11, 5539-5563.

463 Buckles, L.K., Weijers, J.W.H., Verschuren, D., Sinninghe Damsté, J.S., 2014b. Sources of
464 core and intact branched tetraether membrane lipids in the lacustrine

environment: Anatomy of Lake Challa and its catchment, equatorial East Africa. Geochimica et Cosmochimica Acta 140, 106-126.

Colcord, D.E., Cadieux, S.B., Brassell, S.C., Castañeda, I.S., Pratt, L.M., White, J.R., 2015. Assessment of branched GDGTs as temperature proxies in sedimentary records from several small lakes in southwestern Greenland. Organic Geochemistry 82, 33-41.

Dang, X., Xue, J., Yang, H., Xie, S., 2016a. Environmental impacts on the distribution of microbial tetraether lipids in Chinese lakes with contrasting pH: Implications for lacustrine paleoenvironmental reconstructions. Science China Earth Sciences 59, 939-950.

Dang, X., Yang, H., Naafs, B.D.A., Pancost, R.D., Xie, S., 2016b. Evidence of moisture control on the methylation of branched glycerol dialkyl glycerol tetraethers in semi-arid and arid soils. Geochimica et Cosmochimica Acta 189, 24-36.

Das, S.K., Bendle, J., Routh, J., 2012. Evaluating branched tetraether lipid-based palaeotemperature proxies in an urban, hyper-eutrophic polluted lake in South Africa. Organic Geochemistry 53, 45-51.

De Jonge, C., Hopmans, E.C., Stadnitskaia, A., Rijpstra, W.I.C., Hofland, R., Tegelaar, E., Sinninghe Damsté, J.S., 2013. Identification of novel penta-and hexamethylated

483 branched glycerol dialkyl glycerol tetraethers in peat using HPLC–MS^2, GC–MS
484 and GC–SMB-MS. Organic Geochemistry 54, 78-82.

485 De Jonge, C., Hopmans, E.C., Zell, C.I., Kim, J.-H., Schouten, S., Sinninghe Damsté, J.S.,
486 2014a. Occurrence and abundance of 6-methyl branched glycerol dialkyl glycerol
487 tetraethers in soils: Implications for palaeoclimate reconstruction. Geochimica et
488 Cosmochimica Acta 141, 97-112.

489 De Jonge, C., Stadnitskaia, A., Hopmans, E.C., Cherkashov, G., Fedotov, A., Sinninghe
490 Damsté, J.S., 2014b. In situ produced branched glycerol dialkyl glycerol
491 tetraethers in suspended particulate matter from the Yenisei River, Eastern
492 Siberia. Geochimica et Cosmochimica Acta 125, 476-491.

493 De Jonge, C., Stadnitskaia, A., Fedotov, A., Sinninghe Damsté, J.S., 2015a. Impact of
494 riverine suspended particulate matter on the branched glycerol dialkyl glycerol
495 tetraether composition of lakes: The outflow of the Selenga River in Lake Baikal
496 (Russia). Organic Geochemistry 83/84, 241-252.

497 De Jonge, C., Stadnitskaia, A., Hopmans, E.C., Cherkashov, G., Fedotov, A., Streletskaya,
498 I.D., Vasiliev, A.A., Sinninghe Damsté, J.S., 2015b. Drastic changes in the
499 distribution of branched tetraether lipids in suspended matter and sediments
500 from the Yenisei River and Kara Sea (Siberia): Implications for the use of
501 brGDGT-based proxies in coastal marine sediments. Geochimica et

Cosmochimica Acta 165, 200-225.

Günther, F., Thiele, A., Gleixner, G., Xu, B., Yao, T., Schouten, S., 2014. Distribution of bacterial and archaeal ether lipids in soils and surface sediments of Tibetan lakes: implications for GDGT-based proxies in saline high mountain lakes. Organic Geochemistry 67, 19-30.

Hedlund, B.P., Paraiso, J.J., Williams, A.J., Huang, Q., Wei, Y., Dijkstra, P., Hungate, B.A., Dong, H., Zhang, C.L., 2013. Wide distribution of autochthonous branched glycerol dialkyl glycerol tetraethers (bGDGTs) in US Great Basin hot springs. Frontiers in Microbiology 4, 222.

Hopmans, E.C., Weijers, J.W.H., Schefuß, E., Herfort, L., Sinninghe Damsté, J.S., Schouten, S., 2004. A novel proxy for terrestrial organic matter in sediments based on branched and isoprenoid tetraether lipids. Earth and Planetary Science Letters 224, 107-116.

Huguet, C., Hopmans, E.C., Febo-Ayala, W., Thompson, D.H., Sinninghe Damsté, J.S., Schouten, S., 2006. An improved method to determine the absolute abundance of glycerol dibiphytanyl glycerol tetraether lipids. Organic Geochemistry 37, 1036-1041.

Li, F., Zhang, C.L., Wang, S., Chen, Y., Sun, C., Dong, H., Li, W., Klotz, M.G., Hedlund, B.P.,

2014. Production of branched tetraether lipids in Tibetan hot springs: A possible linkage to nitrite reduction by thermotolerant or thermophilic bacteria? Chemical Geology 386, 209-217.

Li, J., Pancost, R.D., Naafs, B.D.A., Yang, H., Zhao, C., Xie, S., 2016. Distribution of glycerol dialkyl glycerol tetraether (GDGT) lipids in a hypersaline lake system. Organic Geochemistry 99, 113-124.

Loomis, S.E., Russell, J.M., Damsté, J.S.S., 2011. Distributions of branched GDGTs in soils and lake sediments from western Uganda: implications for a lacustrine paleothermometer. Organic Geochemistry 42, 739-751.

Loomis, S.E., Russell, J.M., Ladd, B., Street-Perrott, F.A., Sinninghe Damsté, J.S., 2012. Calibration and application of the branched GDGT temperature proxy on East African lake sediments. Earth and Planetary Science Letters 357/358, 277-288.

Loomis, S.E., Russell, J.M., Eggermont, H., Verschuren, D., Sinninghe Damsté, J.S., 2014a. Effects of temperature, pH and nutrient concentration on branched GDGT distributions in East African lakes: Implications for paleoenvironmental reconstruction. Organic Geochemistry 66, 25-37.

Loomis, S.E., Russell, J.M., Heureux, A.M., D'Andrea, W.J., Sinninghe Damsté, J.S., 2014b. Seasonal variability of branched glycerol dialkyl glycerol tetraethers (brGDGTs)

538 in a temperate lake system. Geochimica et Cosmochimica Acta 144, 173-187.

539 Naafs, B.D.A., Pancost, R.D., 2014. Environmental conditions in the South Atlantic
540 (Angola Basin) during the Early Cretaceous. Organic Geochemistry 76, 184-193.

541 Naafs, B.D.A., Gallego-Sala, A.V., Inglis, G.N., Pancost, R.D., 2017a. Refining the global
542 branched glycerol dialkyl glycerol tetraether (brGDGT) soil temperature
543 calibration. Organic Geochemistry 106, 48-56.

544 Naafs, B.D.A., Inglis, G.N., Zheng, Y., Amesbury, M.J., Biester, H., Bindler, R., Blewett, J.,
545 Burrows, M.A., del Castillo Torres, D., Chambers, F.M., Cohen, A.D., Evershed, R.P.,
546 Feakins, S.J., Gałka, M., Gallego-Sala, A., Gandois, L., Gray, D.M., Hatcher, P.G.,
547 Honorio Coronado, E.N., Hughes, P.D.M., Huguet, A., Könönen, M.,
548 Laggoun-Défarge, F., Lähteenoja, O., Lamentowicz, M., Marchant, R., McClymont,
549 E., Pontevedra-Pombal, X., Ponton, C., Pourmand, A., Rizzuti, A.M., Rochefort, L.,
550 Schellekens, J., De Vleeschouwer, F., Pancost, R.D., 2017b. Introducing global
551 peat-specific temperature and pH calibrations based on brGDGT bacterial lipids.
552 Geochimica et Cosmochimica Acta 208, 285-301.

553 Naeher, S., Peterse, F., Smittenberg, R.H., Niemann, H., Zigah, P.K., Schubert, C.J., 2014.
554 Sources of glycerol dialkyl glycerol tetraethers (GDGTs) in catchment soils, water
555 column and sediments of Lake Rotsee (Switzerland) – Implications for the
556 application of GDGT-based proxies for lakes. Organic Geochemistry 66, 164-173.

557 Niemann, H., Stadnitskaia, A., Wirth, S., Gilli, A., Anselmetti, F., Sinninghe Damsté, J.,
558 Schouten, S., Hopmans, E., Lehmann, M., 2012. Bacterial GDGTs in Holocene
559 sediments and catchment soils of a high Alpine lake: application of the
560 MBT/CBT-paleothermometer. Climate of the Past 8, 889-906.

561 Pearson, E.J., Juggins, S., Talbot, H.M., Weckström, J., Rosén, P., Ryves, D.B., Roberts, S.J.,
562 Schmidt, R., 2011. A lacustrine GDGT-temperature calibration from the
563 Scandinavian Arctic to Antarctic: renewed potential for the application of
564 GDGT-paleothermometry in lakes. Geochimica et Cosmochimica Acta 75,
565 6225-6238.

566 Peterse, F., van der Meer, J., Schouten, S., Weijers, J.W., Fierer, N., Jackson, R.B., Kim, J.-H.,
567 Sinninghe Damsté, J.S., 2012. Revised calibration of the MBT–CBT
568 paleotemperature proxy based on branched tetraether membrane lipids in
569 surface soils. Geochimica et Cosmochimica Acta 96, 215-229.

570 Schoon, P.L., de Kluijver, A., Middelburg, J.J., Downing, J.A., Sinninghe Damsté, J.S.,
571 Schouten, S., 2013. Influence of lake water pH and alkalinity on the distribution
572 of core and intact polar branched glycerol dialkyl glycerol tetraethers (GDGTs) in
573 lakes. Organic Geochemistry 60, 72-82.

574 Schouten, S., Hopmans, E.C., Pancost, R.D., Sinninghe Damsté, J.S., 2000. Widespread
575 occurrence of structurally diverse tetraether membrane lipids: evidence for the

ubiquitous presence of low-temperature relatives of hyperthermophiles. Proceedings of the National Academy of Sciences USA 97, 14421-14426.

Schouten, S., Hopmans, E.C., Sinninghe Damsté, J.S., 2013. The organic geochemistry of glycerol dialkyl glycerol tetraether lipids: A review. Organic Geochemistry 54, 19-61.

Shanahan, T.M., Hughen, K.A., Van Mooy, B.A.S., 2013. Temperature sensitivity of branched and isoprenoid GDGTs in Arctic lakes. Organic Geochemistry 64, 119-128.

Sinninghe Damsté, J.S., Hopmans, E.C., Pancost, R.D., Schouten, S., Geenevasen, J.A., 2000. Newly discovered non-isoprenoid glycerol dialkyl glycerol tetraether lipids in sediments. Chemical Communications, 1683-1684.

Sinninghe Damsté, J.S., Schouten, S., Hopmans, E.C., van Duin, A.C., Geenevasen, J.A., 2002. Crenarchaeol: the characteristic core glycerol dibiphytanyl glycerol tetraether membrane lipid of cosmopolitan pelagic crenarchaeota. Journal of Lipid Research 43, 1641-1651.

Sinninghe Damsté, J.S., Ossebaar, J., Abbas, B., Schouten, S., Verschuren, D., 2009. Fluxes and distribution of tetraether lipids in an equatorial African lake: constraints on the application of the TEX_{86} palaeothermometer and BIT index in lacustrine

settings. Geochimica et Cosmochimica Acta 73, 4232-4249.

Sinninghe Damsté, J.S., Rijpstra, W.I.C., Hopmans, E.C., Weijers, J.W.H., Foesel, B.U., Overmann, J., Dedysh, S.N., 2011. 13,16-Dimethyl octacosanedioic acid (iso-diabolic acid), a common membrane-spanning lipid of *Acidobacteria* Subdivisions 1 and 3. Applied and Environmental Microbiology 77, 4147-4154.

Sinninghe Damsté, J.S., Ossebaar, J., Schouten, S., Verschuren, D., 2012. Distribution of tetraether lipids in the 25-ka sedimentary record of Lake Challa: extracting reliable TEX_{86} and MBT/CBT palaeotemperatures from an equatorial African lake. Quaternary Science Reviews 50, 43-54.

Sinninghe Damsté, J.S., Rijpstra, W.I.C., Hopmans, E.C., Foesel, B.U., Wüst, P.K., Overmann, J., Tank, M., Bryant, D.A., Dunfield, P.F., Houghton, K., Stott, M.B., 2014. Ether- and ester-bound iso-siabolic acid and other lipids in members of *Acidobacteria* subdivision 4. Applied and Environmental Microbiology 80, 5207-5218.

Sun, Q., Chu, G., Liu, M., Xie, M., Li, S., Ling, Y., Wang, X., Shi, L., Jia, G., Lü, H., 2011. Distributions and temperature dependence of branched glycerol dialkyl glycerol tetraethers in recent lacustrine sediments from China and Nepal. Journal of Geophysical Research: Biogeosciences 116(G1), G01008.

Tierney, J.E., Russell, J.M., 2009. Distributions of branched GDGTs in a tropical lake

612 system: Implications for lacustrine application of the MBT/CBT paleoproxy.
613 Organic Geochemistry 40, 1032-1036.

614 Tierney, J.E., Russell, J.M., Eggermont, H., Hopmans, E., Verschuren, D., Sinninghe Damsté,
615 J.S., 2010. Environmental controls on branched tetraether lipid distributions in
616 tropical East African lake sediments. Geochimica et Cosmochimica Acta 74,
617 4902-4918.

618 Tierney, J.E., Schouten, S., Pitcher, A., Hopmans, E.C., Sinninghe Damsté, J.S., 2012. Core
619 and intact polar glycerol dialkyl glycerol tetraethers (GDGTs) in Sand Pond,
620 Warwick, Rhode Island (USA): insights into the origin of lacustrine GDGTs.
621 Geochimica et Cosmochimica Acta 77, 561-581.

622 Wang, H., Liu, W., Zhang, C.L., Wang, Z., Wang, J., Liu, Z., Dong, H., 2012. Distribution of
623 glycerol dialkyl glycerol tetraethers in surface sediments of Lake Qinghai and
624 surrounding soil. Organic Geochemistry 47, 78-87.

625 Wang, M., Liang, J., Hou, J., Hu, L., 2016. Distribution of GDGTs in lake surface sediments
626 on the Tibetan Plateau and its influencing factors. Science China Earth Sciences
627 59, 961-974.

628 Weber, Y., De Jonge, C., Rijpstra, W.I.C., Hopmans, E.C., Stadnitskaia, A., Schubert, C.J.,
629 Lehmann, M.F., Sinninghe Damsté, J.S., Niemann, H., 2015. Identification and

carbon isotope composition of a novel branched GDGT isomer in lake sediments: Evidence for lacustrine branched GDGT production. Geochimica et Cosmochimica Acta 154, 118-129.

Weijers, J.W.H., Schouten, S., Hopmans, E.C., Geenevasen, J.A.J., David, O.R.P., Coleman, J.M., Pancost, R.D., Sinninghe Damsté, J.S., 2006a. Membrane lipids of mesophilic anaerobic bacteria thriving in peats have typical archaeal traits. Environmental Microbiology 8, 648-657.

Weijers, J.W.H., Schouten, S., Spaargaren, O.C., Sinninghe Damsté, J.S., 2006b. Occurrence and distribution of tetraether membrane lipids in soils: Implications for the use of the TEX_{86} proxy and the BIT index. Organic Geochemistry 37, 1680-1693.

Weijers, J.W.H., Schouten, S., van den Donker, J.C., Hopmans, E.C., Sinninghe Damsté, J.S., 2007. Environmental controls on bacterial tetraether membrane lipid distribution in soils. Geochimica et Cosmochimica Acta 71, 703-713.

Woltering, M., Werne, J.P., Kish, J.L., Hicks, R., Sinninghe Damsté, J.S., Schouten, S., 2012. Vertical and temporal variability in concentration and distribution of thaumarchaeotal tetraether lipids in Lake Superior and the implications for the application of the TEX_{86} temperature proxy. Geochimica et Cosmochimica Acta 87, 136-153.

Woltering, M., Atahan, P., Grice, K., Heijnis, H., Taffs, K., Dodson, J., 2014. Glacial and Holocene terrestrial temperature variability in subtropical east Australia as inferred from branched GDGT distributions in a sediment core from Lake McKenzie. Quaternary Research 82, 132-145.

Xiao, W., Xu, Y., Ding, S., Wang, Y., Zhang, X., Yang, H., Wang, G., Hou, J., 2015. Global calibration of a novel, branched GDGT-based soil pH proxy. Organic Geochemistry 89/90, 56-60.

Yang, H., Pancost, R.D., Dang, X., Zhou, X., Evershed, R.P., Xiao, G., Tang, C., Gao, L., Guo, Z., Xie, S., 2014. Correlations between microbial tetraether lipids and environmental variables in Chinese soils: Optimizing the paleo-reconstructions in semi-arid and arid regions. Geochimica et Cosmochimica Acta 126, 49-69.

Yang, H., Lü, X., Ding, W., Lei, Y., Dang, X., Xie, S., 2015. The 6-methyl branched tetraethers significantly affect the performance of the methylation index (MBT') in soils from an altitudinal transect at Mount Shennongjia. Organic Geochemistry 82, 42-53.

Zell, C., Kim, J.-H., Moreira-Turcq, P., Abril, G., Hopmans, E.C., Bonnet, M.-P., Sobrinho, R.L., Sinninghe Damsté, J.S., 2013. Disentangling the origins of branched tetraether lipids and crenarchaeol in the lower Amazon River: Implications for GDGT‐based proxies. Limnology and Oceanography 58, 343-353.

667 Zhang, C.L., Wang, J., Dodsworth, J.A., Williams, A.J., Zhu, C., Hinrichs, K.-U., Zheng, F.,
668 Hedlund, B.P., 2013. In situ production of branched glycerol dialkyl glycerol
669 tetraethers in a great basin hot spring (USA). Frontiers in microbiology 4, 131.

670 Zheng, X., Zhang, M., Dong, J., Gao, Z., Xu, C., Han, Z., Zhang, B., Sun, D., Wang, K., 1992.
671 Salt Lakes in Inner Mongolia. Science Press, Beijing, China (in Chinese).

672 Zheng, X., Zhang, M., Li, B., Xu, C., 2002. Salt lakes of China. Science Press, Beijing, China
673 (in Chinese)

674

675

676 Figure Captions

677 **Fig.1.** Structures of 5-Me and 6-Me brGDGTs, and crenarchaeol. The 6-Me brGDGTs
678 are numbered with an accent after the Roman numerals of the corresponding 5-Me
679 brGDGTs. The structures of the hexa- and pentamethylated brGDGTs with cyclopentyl
680 moiety(ies) IIb', IIc', IIIb' and IIIc' are tentatively assigned.

681 **Fig.2.** Map for 11 ponds in New Barag Left Banner (Inner Mongolia), with sampling
682 sites indicated.

683 **Fig.3.** Fractional abundance of individual brGDGTs and isomers in surface sediments
684 and soils.

685 **Fig.4.** Relationship between salinity and difference in brGDGT concentration in
686 surface sediments and soils.

687 **Fig.5.** Cross plots of MBT' and CBT, MBT'_{5ME} and CBT'_{5ME}, and MBT'_{6ME} and CBT'_{6ME} for
688 surface sediments and soils from the 11 eleven ponds.

689 **Fig.6.** Cross plots, comparing isomer ratios (IRs) of IIIa' and IIa' in surface sediments
690 and soils: (a) $IR_{IIIa'}$ for surface sediments vs. corresponding soils; (b) $IR_{IIa'}$ in surface
691 sediments vs. corresponding soils; (c) $IR_{IIIa'}$ vs. $IR_{IIa'}$ for surface sediments; and (d) $IR_{IIIa'}$
692 vs. $IR_{IIa'}$ for soils (1:1 ratio, dashed line).

693 **Fig.7.** Redundancy analysis triplots showing relationships between water chemical
694 parameters and (a) individual brGDGTs and (b) brGDGT-based indices (numbers on
695 plots refer to corresponding samples in Table 1).

696 Figure 1

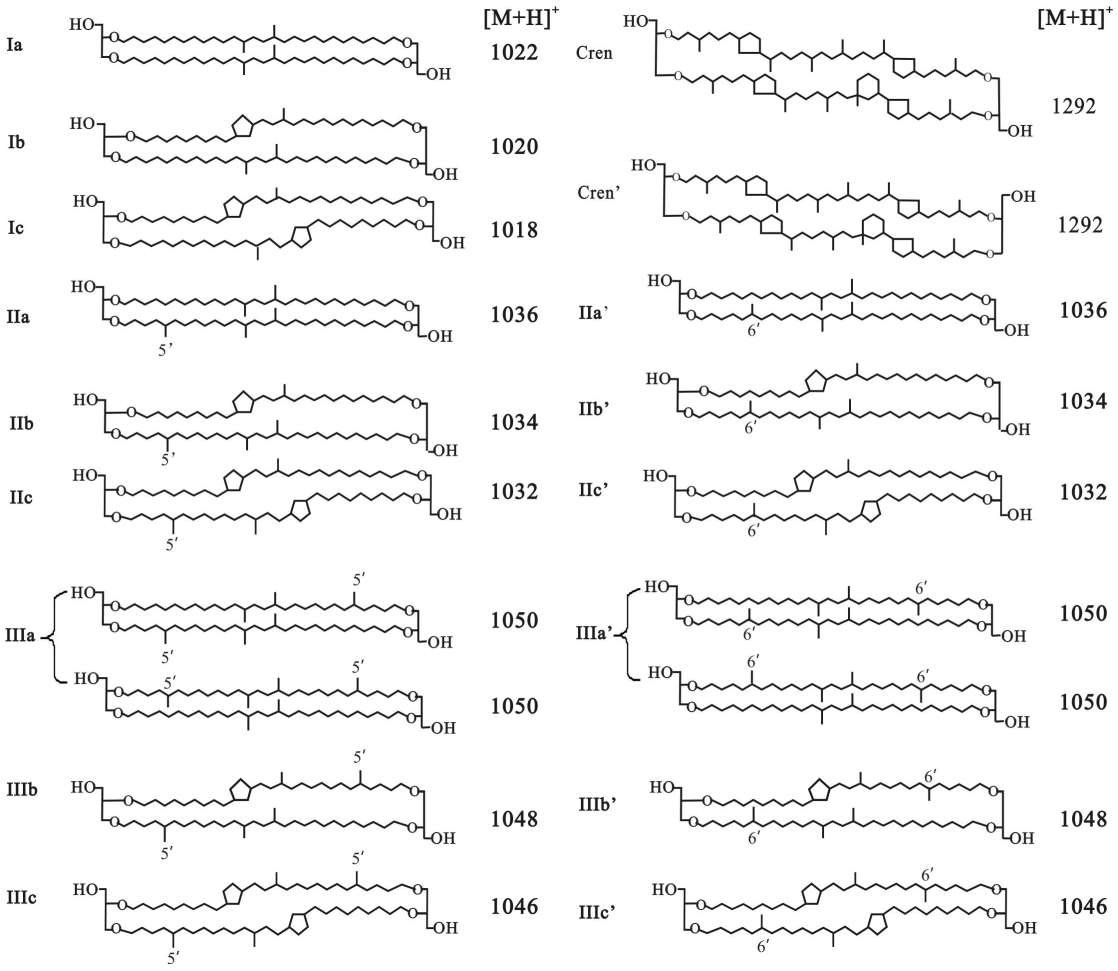

697

698 Figure 2

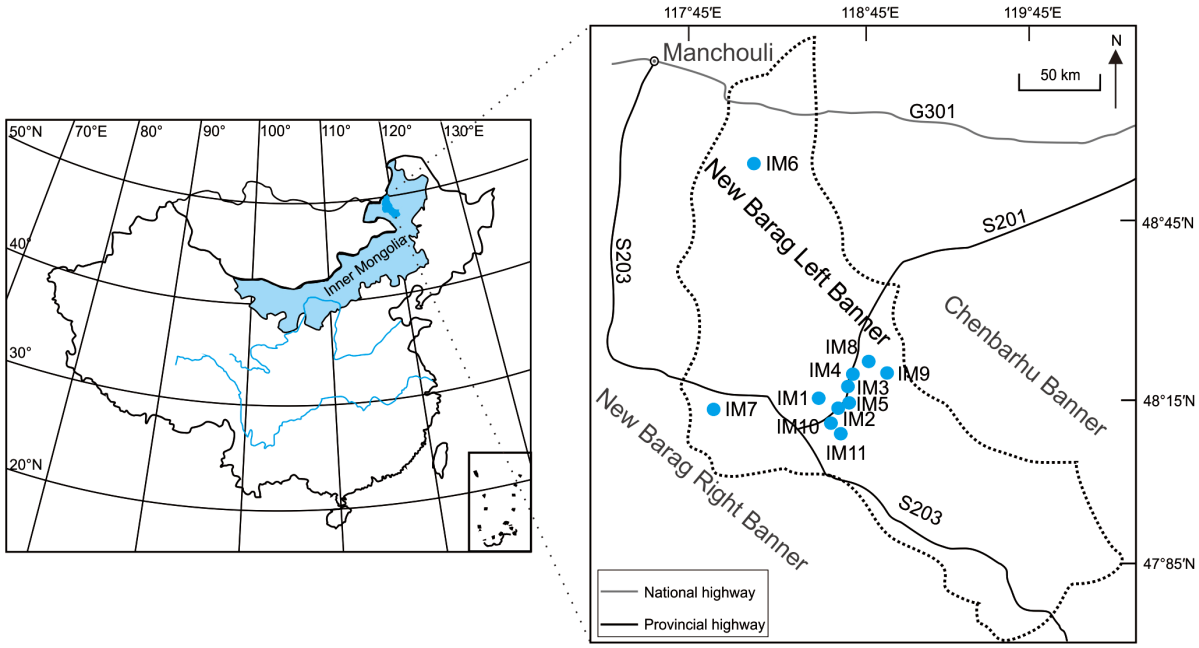

699

700 Figure 3

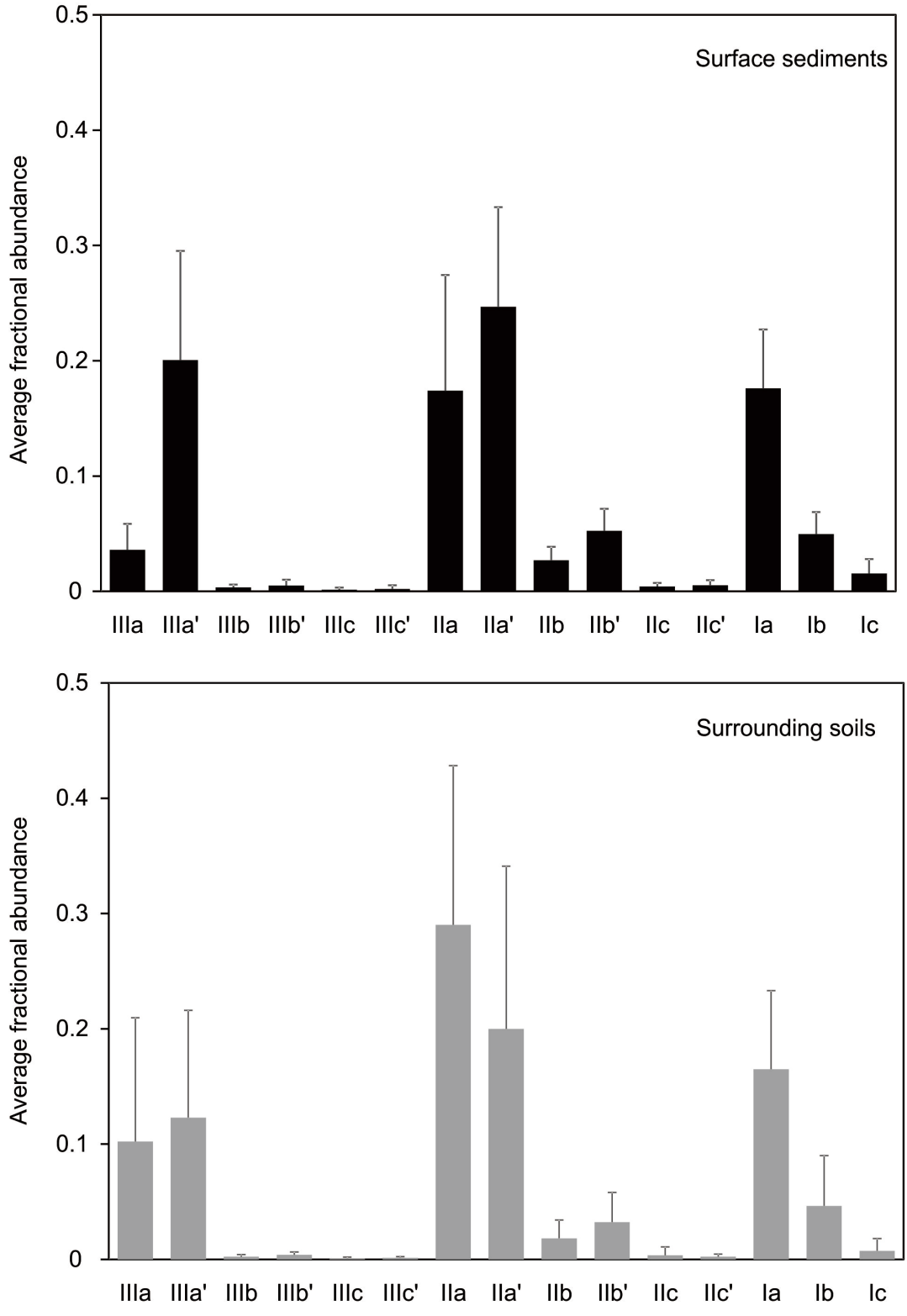

701

702 Figure 4

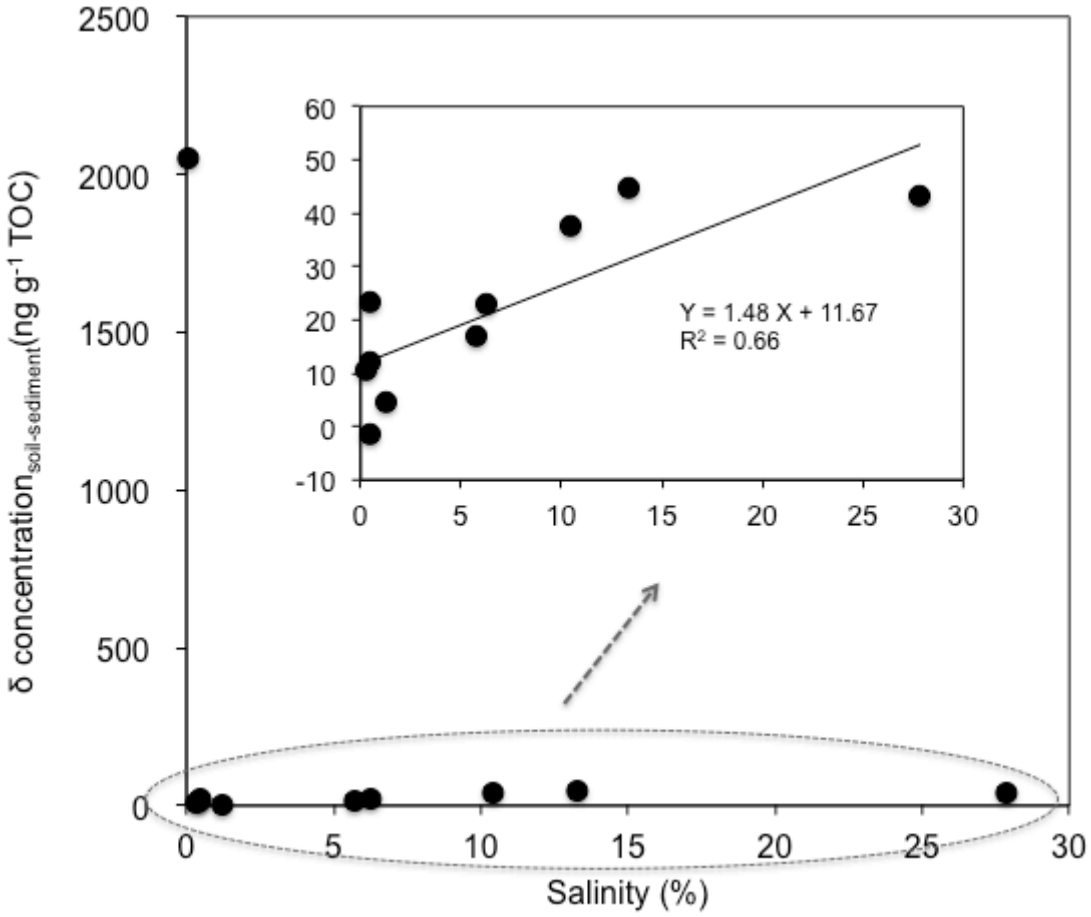

703

704 Figure 5

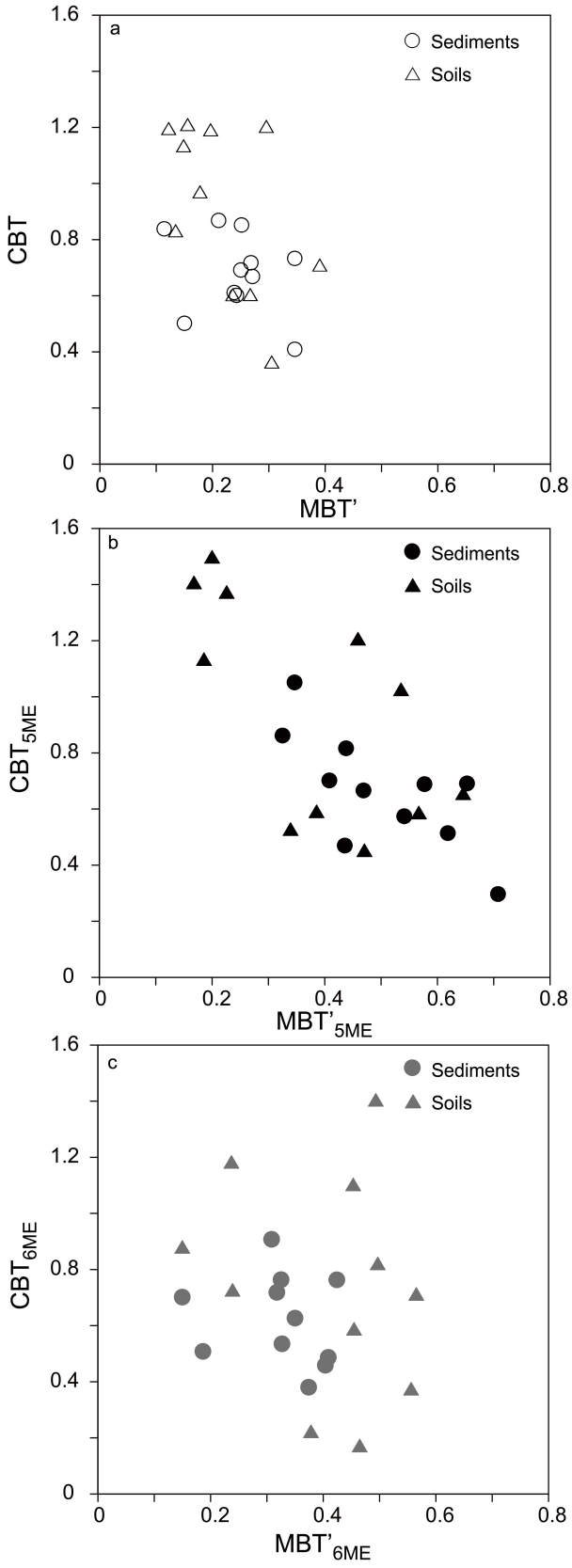

705

706 Figure 6

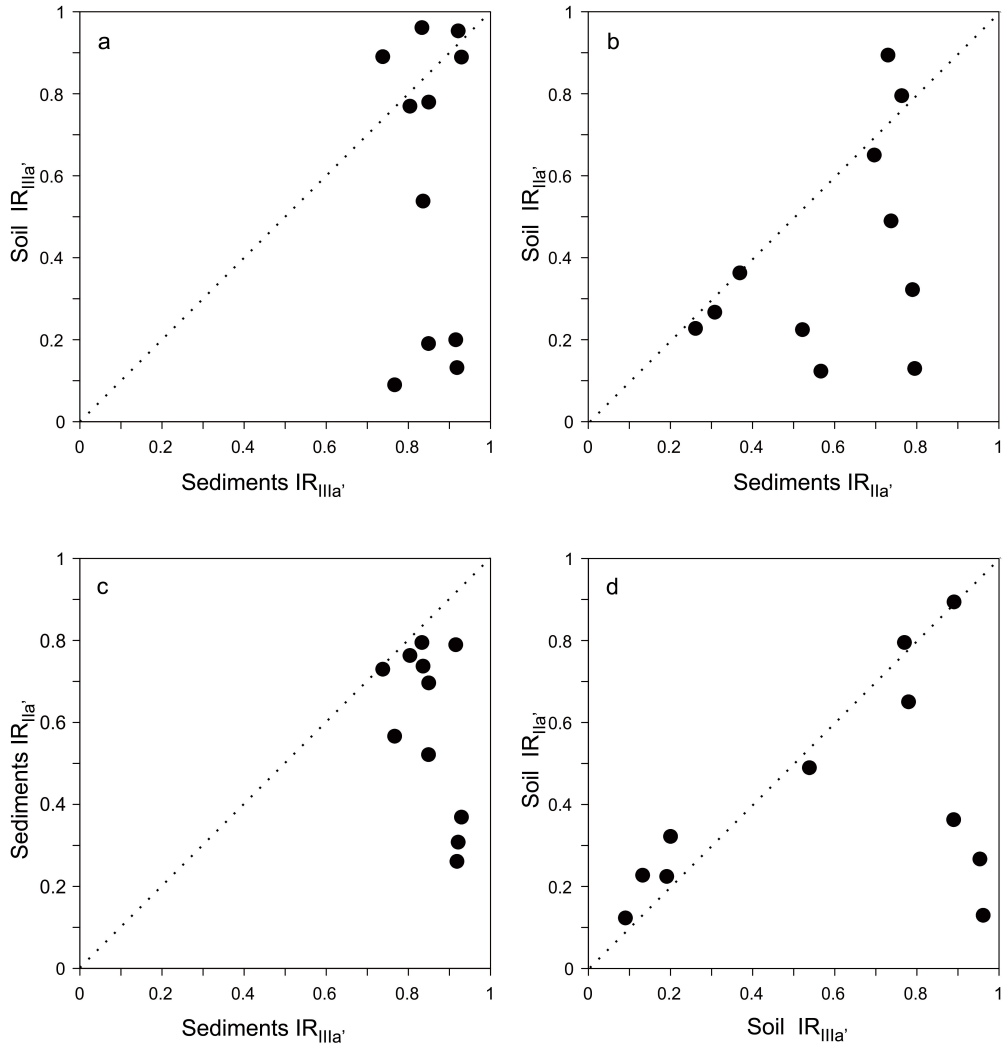

707

708 Figure 7

709

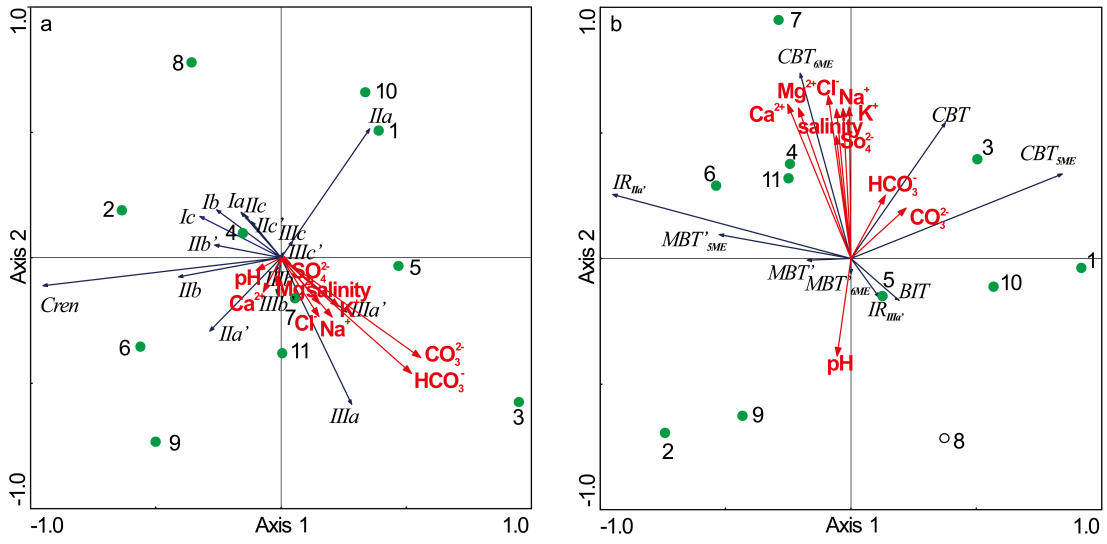

710

Tables

Table 1

Information for the 11 ponds in New Barag Left Banner (Inner Mongolia; n.d., not determined).

ID	Location	Altitude (m)	Depth (m)	Area (km^2)	pH	Salinity (%)	Na^+ (mg/l)	K^+ (mg/l)	Mg^{2+} (mg/l)	Ca^{2+} (mg/l)	Cl^- (mg/l)	SO_4^{2-} (mg/l)	HCO_3^- (mg/l)	CO_3^{2-} (mg/l)
IM1	48°15.114' N; 118°25.102' E	685	0.2	2	9.3	0.42	1400	30	16	0	1200	800	620	140
IM2	48°14.557' N; 118°26.564' E	682	0.2	n.d.	10	1.22	4400	30	15	0	2340	1360	1700	2350
IM3	48°18.785' N; 118°32.166' E	658	0.3	1.8	9.7	13.3	43000	160	70	0	46200	24200	5700	14000
IM4	48°18.850' N; 118°32.872' E	671	0.2	n.d.	9.8	0.5	1600	10	25	0	1200	800	760	500
IM5	48°14.922' N; 118°27.864' E	675	0.2	2	8.6	0.08	90	0	40	2	270	n.d.	330	40
IM6	48°53.214' N; 118°05.653' E	545	0.3	3.1	9.1	5.74	18000	30	1500	90	26000	11300	250	290
IM7	48°16.734' N; 117°39.334' E	565	0.2	n.d.	7.7	27.87	66000	306	12000	340	100000	98600	1130	n.d.
IM8	48°23.130' N; 118°42.539' E	657	0.5	7	8.8	10.43	27600	90	670	20	30000	44900	500	240
IM9	48°22.700' N; 118°49.277' E	678	0.2	1.6	9.4	0.32	900	26	30	n.d.	640	220	1000	350
IM10	48°12.591' N; 118°25.237' E	683	0.2	1.2	9.3	0.44	1460	25	50	n.d.	1120	630	780	320
IM11	48°10.722' N; 118°26.041' E	665	0.5	3.8	9.3	6.23	19000	70	20	n.d.	24000	14800	2400	1980